POLITECNICO DI TORINO
Repository ISTITUZIONALE

Spatial activation of motor evoked potentials depends on paired-pulse transcranial magnetic stimulation orientation and intensity

Original
Spatial activation of motor evoked potentials depends on paired-pulse transcranial magnetic stimulation orientation and intensity / Parvin, S., Juurakko, J., Sinisalo, H., Cerone, G.L., Botter, A., Ilmoniemi, R.J., Piitulainen, H., Souza, V.H.. - In: CLINICAL NEUROPHYSIOLOGY. - ISSN 1388-2457. - STAMPA. - 183:(2026). [10.1016/j.clinph.2025.2111477]

Availability:
This version is available at: 11583/3010770 since: 2026-05-12T08:54:27Z

Publisher:
Elsevier

Published
DOI:10.1016/j.clinph.2025.2111477

Terms of use:

This article is made available under terms and conditions as specified in the corresponding bibliographic description in the repository

Publisher copyright

(Article begins on next page)

19 November 2026

Clinical Neurophysiology 183 (2026) 2111477

Contents lists available at ScienceDirect

Clinical Neurophysiology

journal homepage: www.elsevier.com/locate/clinph

Spatial activation of motor evoked potentials depends on paired-pulse transcranial magnetic stimulation orientation and intensity

Shokoofeh Parvin [a,*], Joona Juurakko [b], Heikki Sinisalo [a], Giacinto L. Cerone [c], Alberto Botter [c], Risto J. Ilmoniemi [a], Harri Piitulainen [b,1], Victor H. Souza [a,1]

[a] Department of Neuroscience and Biomedical Engineering, Aalto University School of Science, Espoo, Finland
[b] Faculty of Sport and Health Sciences, University of Jyväskylä, Jyväskylä, Finland
[c] LISiN, Department of Electronics and Telecommunications, Politecnico di Torino, Turin, Italy

ARTICLE INFO

Keywords:
Spatial muscle recruitment
Paired-pulse stimulation
Intracortical facilitation
Motor control
Muscle imaging
Short-interval intracortical inhibition
Multi-coil TMS

ABSTRACT

Objective: To investigate how stimulus orientation, intensity, and interstimulus interval (ISI) in paired-pulse transcranial magnetic stimulation (TMS) influence the spatial activation of motor evoked potentials (MEPs) in forearm flexor muscles.

Methods: Paired-pulse paradigms were applied to the motor cortex using multi-coil TMS (mTMS) to control the stimulus parameters electronically without coil repositioning. MEP spatial activation was recorded with a high-density surface electromyography (HDsEMG) grid over the forearm muscles. Conditioning stimuli (CS) were delivered at anterior-to-medial (0°) and posterior-to-medial (90°) orientations and 70–90 % of resting motor threshold (rMT), followed by test stimuli (TS) at 0° and 110 % rMT. ISIs of 0.5 and 8 ms probed neuronal refractoriness and intracortical facilitation, respectively.

Results: MEPs were facilitated at 8-ms and suppressed at 0.5-ms ISI. At 0.5 ms, changing CS orientation from 0° to 90° reduced suppression. Increasing CS intensity shifted activation centroids medially in most cases. Centroids were more medial at 8 ms and more lateral at 0.5 ms.

Conclusions: TMS pulse orientation, intensity, and ISI systematically affect the magnitude and spatial activation of forearm muscles.

Significance: Our findings highlight the utility of mTMS–HDsEMG in probing neurophysiological mechanisms of corticomotor control with important diagnostic and therapeutic clinical implications.

1. Introduction

Transcranial magnetic stimulation (TMS) is a useful non-invasive tool for probing cortical excitability and motor function (Barker et al., 1985). The TMS technique involves applying a magnetic pulse that induces an electric field (E-field) in the cortical tissue. This E-field depolarizes neuronal populations and leads to motor-evoked potentials (MEPs) in the peripheral muscles if applied over the primary motor cortex. These MEPs offer evidence of the functions of the corticospinal pathway (Rossini et al., 2015), such as demyelination in multiple sclerosis (Hess et al., 1987), cortical excitability and motor pathway integrity post-stroke (Stinear et al., 2012), and altered corticospinal recruitment and facilitation in incomplete spinal cord injury (Davey et al., 1999).

A critical factor influencing TMS outcomes is the orientation of the induced current. Studies have shown that altering coil orientation affects the recruitment of different neuronal populations and modulates both excitatory and inhibitory circuits (Chen et al., 2003; Souza et al., 2022; Souza et al., 2025; Tugin et al., 2021; Volz et al., 2015; Ziemann et al., 1996). Anterior-to-posterior (AP) versus posterior-to-anterior (PA) currents, for example, activate distinct inputs to pyramidal neurons, affecting the timing and nature of I-waves and intracortical inhibition (Fong et al., 2021; Hamada et al., 2013). Ziemann et al. (1996) and Souza et al. (2025) further demonstrated that intracortical facilitation (ICF) is highly sensitive to current direction, whereas inhibition is less so, suggesting different orientation dependencies for excitatory and

* Corresponding author at: Department of Neuroscience and Biomedical Engineering, Aalto University School of Science, Rakentajanaukio 2, 02150 Espoo, Finland.
E-mail address: shokoofeh.parvin@aalto.fi (S. Parvin).
[1] Co-senior authors.

https://doi.org/10.1016/j.clinph.2025.2111477
Accepted 8 December 2025
Available online 10 December 2025
1388-2457/© 2025 The Authors. Published by Elsevier B.V. on behalf of International Federation of Clinical Neurophysiology. This is an open access article under the CC BY license (http://creativecommons.org/licenses/by/4.0/).

inhibitory pathways.

Most paired-pulse TMS studies have focused on intrinsic hand muscles (Kujirai et al., 1993; Nikolov et al., 2021; Säisänen et al., 2011), leaving the cortical control of forearm flexor muscles comparatively underexplored. This gap is notable, given that forearm muscles are essential for hand and wrist function, and their somatotopic representations may differ in organization and sensitivity to TMS conditions.

Paired-pulse TMS, in which a subthreshold conditioning stimulus (CS) precedes a suprathreshold test stimulus (TS), enables the study of intracortical excitability mechanisms. Short interstimulus intervals (ISIs; $\leq$1 ms) often produce suppression via neuronal refractoriness (Hanajima et al., 1998; Roshan et al., 2003; Souza et al., 2025), whereas longer ISIs (7–15 ms) typically reflect ICF mediated by excitatory circuits and N-Methyl-D-aspartic (NMDA) receptor activity (Schwenkreis et al., 1999; Souza et al., 2025; Ziemann et al., 1998a). Although these mechanisms have been well characterized in hand muscles, their anatomical and functional expression in forearm muscles remains poorly understood.

High-density surface electromyography (HDsEMG) offers unique advantages for studying the spatial domain of muscle activation. Its high spatial resolution allows for detailed mapping of motor unit recruitment, identification of activation hotspots, and separation of overlapping responses in adjacent muscles (Gallina and Botter, 2013; Merletti et al., 2010). When combined with TMS, HDsEMG enables high-resolution spatial and temporal characterization of muscle responses (Del Vecchio et al., 2019; Souza et al., 2018b; van Elswijk et al., 2008). Prior work has demonstrated its utility in differentiating MEPs across neighboring muscle groups (Jiang et al., 2021; Neva et al., 2017) and in mapping activation topographies (Souza et al., 2018b; van Elswijk et al., 2008).

Despite these advances, the spatial effects of orientation-dependent paired-pulse stimulation on forearm flexor muscle activation remain poorly understood. Previous studies have shown that induced current direction (e.g., anterior-to-medial vs. posterior-to-medial) can significantly influence MEP modulation (Bashir et al., 2013; D'Ostilio et al., 2016; Gomez-Tames et al., 2018; Kaneko et al., 1996; Souza et al., 2025; Tugin et al., 2021), but these findings have been limited to intrinsic hand muscles and conventional EMG measuring a single MEP.

In the present study, we integrated multi-coil TMS (mTMS), a novel system enabling electronic control of stimulus orientation without coil repositioning (Souza et al., 2022), with HDsEMG to assess spatial and amplitude-based modulation of MEPs in forearm flexors. This setup enables precise evaluation of how different CS orientations and intensities affect corticospinal output across both ultra-short (0.5 ms) and intermediate (8 ms) ISIs, providing insights into mechanisms of neuronal refractoriness and facilitation (Nieminen et al., 2019; Tugin et al., 2021; Souza et al., 2025). Furthermore, by tracking shifts in the centroid of muscle activation maps, we can probe the spatial reorganization of muscle activity across stimulation conditions.

This study aimed to investigate how paired-pulse stimulation conditions, specifically CS orientation and intensity and ISI, modulate the spatial distribution and magnitude of MEPs in forearm flexor muscles. By combining mTMS with HDsEMG, we aimed to map MEP spatial patterns in response to different cortical stimulation conditions. We hypothesize that variations in TMS stimulus conditions will result in distinct patterns of MEP facilitation or suppression, as well as spatial shifts in muscle activation maps, reflecting the differential recruitment of cortical circuits.

2. Methods

2.1. Participants

Twelve healthy subjects (five females, nine right-handed (Oldfield, 1971), age: 30.4 $\pm$ 8.6) participated in the study with a fully crossed and within-subject experimental design. The participants' details are given in Supplementary Table 1. All participants gave written informed consent before the experiment. The study was performed in accordance with the Declaration of Helsinki and approved by the Coordinating Ethics Committee of the Hospital District of Helsinki and Uusimaa (number HUS/1198/2016).

2.2. Experimental procedure

We utilized a custom-made mTMS system with a coil set comprising two perpendicular figure-of-eight coils (Souza et al., 2022). This system allows sub-millisecond and 1°-resolution electronic control of the induced E-field orientation. This electronic control is achieved without mechanical movement of the coil set by superimposing the induced E-field of each overlapping coil.

Subjects were instructed to sit relaxed on a reclining chair. To identify the stimulation hotspot and determine the resting motor threshold (rMT) of the flexor carpi radialis (FCR) muscle, we initially used a single-channel pseudo-monopolar EMG configuration. EMG electrodes (Neuroline 700, Model 70001-K/12, Ambu A/S, Denmark) were placed over the FCR and extensor digitorum communis (EDC) muscles after the skin was abraded with sandpaper and cleaned with 80 % alcohol. The reference electrode was placed on the medial epicondyle, and the active electrode over the FCR innervation zone, approximately one-third of the distance between the medial epicondyle and the styloid process of the radius (Barbero et al., 2012). EMG signals were recorded using a Nexstim eXimia EMG device (3000-Hz sampling frequency; 10–500 Hz band-pass filter; Nexstim Plc).

To locate the hotspot, the mTMS coil array was positioned over the hand knob of the left primary motor cortex and adjusted to evoke the strongest and most consistent MEPs on the FCR muscle, such that a 0° stimulus orientation induced an E-field perpendicular to the central sulcus and in the PA direction. At the hostpot, the rMT was measured at 0° and 90° stimulus orientations using an in-house MATLAB implementation of the threshold hunting algorithm described by Awiszus (2003). Coil placement was guided by a neuronavigation system (NBS 3, Nexstim Plc) using each subject's individual T1-weighted anatomical MRI (1-mm isotropic voxels).

Once the hotspot and rMT were established, the conventional EMG electrodes were removed, and a 32-channel HDsEMG grid (4 rows $\times$ 8 columns; inter-electrode distance = 1 cm) was positioned so that the intersection between rows 2–3 and columns 3–4 was centered over the same FCR location used for hotspot and rMT identification with the conventional EMG electrode, shown in Fig. 1. Signals were recorded in a monopolar configuration, using each electrode referenced to a common ground (placed on the medial epicondyle). The HDsEMG covered the following superficial flexor muscles from lateral to medial: FCR, palmaris longus (PL), and flexor carpi ulnaris (FCU). HDsEMG signals were bandpass filtered between 10–500 Hz, amplified with a gain of 183 $\pm$ 1 V/V, digitized at 2048 Hz using a 16-bit A/D converter, and transmitted wirelessly for real-time synchronization, monitoring, and storage using the MEACS system (ReC Bioengineering Laboratories and LISiN, Politecnico di Torino, Italy; (Cerone et al., 2019; Cerone et al., 2022)).

To examine the effects of neuronal refractoriness and ICF on the spatial activation of the forearm flexor muscles, we conducted two distinct paired-pulse protocols. For probing neuronal refractoriness, we employed an ISI of 0.5 ms, and for probing ICF, we utilized an ISI of 8 ms. For each ISI, we assessed the following CS intensities: 70 %, 80 %, and 90 % of the rMT for both 0° anterior-to-medial and 90° posterior-to-medial orientations. The TS intensity was fixed at 110 % rMT for the 0° orientation. The TS intensity (110 % rMT) was selected to ensure a more focal cortical activation (i.e., reduced current spread and overlap of motor representations) (Tardelli et al., 2022; van de Ruit and Grey, 2016) and to increase sensitivity to stimulus-orientation effects (Souza et al., 2022; Souza et al., 2025). This intensity corresponds to approximately 145 % aMT (Ma et al., 2023) and elicits complete I-wave patterns in descending volleys (Di Lazzaro et al., 2001), suitable for assessing

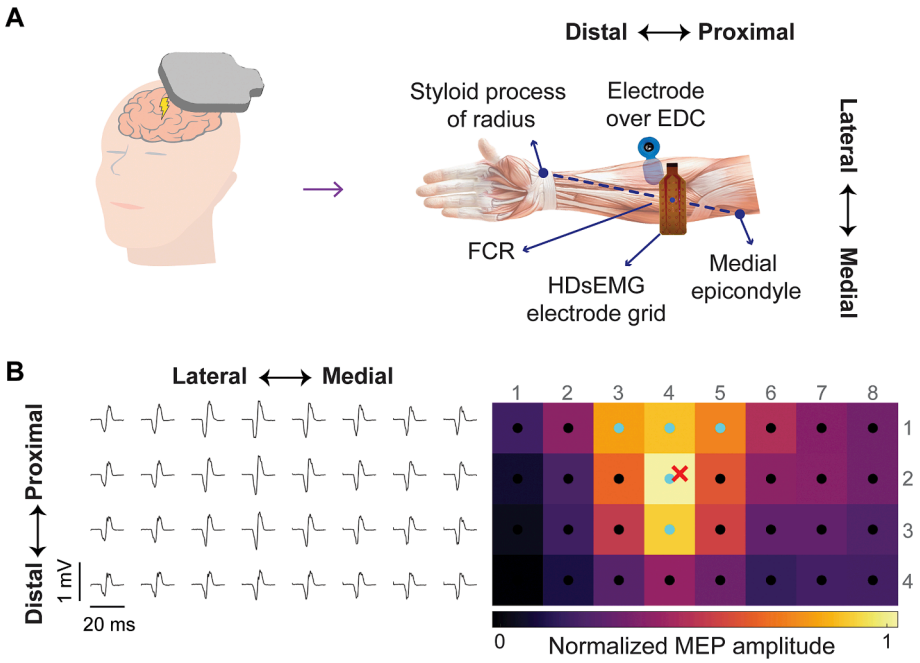


Fig. 1. Schematic illustration of the mTMS–HDsEMG experimental setup. A) Placement of the HDsEMG grid over the forearm flexor muscles. B) Representative example of monopolar MEPs recorded with the HDsEMG grid (left) and the corresponding spatial distribution of peak-to-peak amplitudes (right). Channels exhibiting 70 % or more of the maximum MEP amplitude within the grid are denoted with blue dots. The centroid of these channels is indicated by the red cross (×). FCR: flexor carpi radialis, EDC: extensor digitorum communis, MEP: motor evoked potential. (For interpretation of the references to colour in this figure legend, the reader is referred to the web version of this article.)

short-interval intracortical inhibition (SICI) and ICF (Chen et al., 1998). For the CS orientation 0°, the coil was positioned approximately perpendicular to the central sulcus on the hotspot of each subject to provide maximal MEP amplitudes, as in our previous studies (Souza et al., 2022; Souza et al., 2025; Tervo et al., 2022). This approach differs from the 45° orientation relative to the midline that is typically adopted in conventional non-navigated single-coil excitability studies (Rossini et al., 2015). However, accounting for individual differences in cortical gyrification and optimizing the E-field alignment with neuronal populations enhances spatial specificity and orientation sensitivity (Fox et al., 2004; Laakso et al., 2014; Opitz et al., 2013, Souza et al., 2022; Weise et al., 2023). We applied 20 stimuli for each of the 12 unique parameter combinations, illustrated in Fig. 2.

A total of 240 paired pulses were given in a pseudo-randomized order, divided into four blocks of 60 pulses each, with each block lasting for about 5 min. In addition, 10 single pulses with an intensity of 110 % of the rMT were measured as a reference for unconditioned MEP.

The required stimulation intensity for Sub05 at CS orientation of 90° was 133 V/m, which surpassed the mTMS device's maximum stimulation intensity (129 V/m). In addition, Sub02 did not have any MEPs at the CS orientation of 90°. Therefore, we utilized the maximum available intensity for them, which was 97 % of the actual threshold for Sub05.

Single pulses had a trapezoidal monophasic current waveform characterized by rising, holding, and falling phases lasting 60.0, 30.0, and 44.2 μs, respectively (Souza et al., 2022). In paired-pulse stimulation, the stimulus intensity was obtained by adjusting the duration of the rise and decay phase for each pulse, as outlined in the method described in (Nieminen et al., 2019; Souza et al., 2025). The waveform durations were determined based on a model of neuronal depolarization during mTMS pulses, taking into account the capacitor voltage drop from the CS and a reference neuronal membrane time constant of 200 μs (Barker et al., 1991; Koponen et al., 2018). The phase durations for the CS were

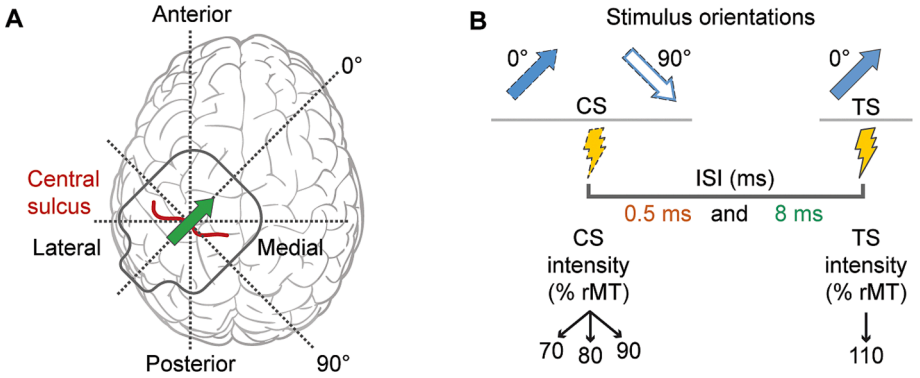


Fig. 2. Schematic representation of the experimental protocol. A) Placement of the mTMS coil array over the head. The green arrow indicates the peak induced E-field orientation relative to the central sulcus. B) The CS was delivered at 0° and 90° orientations, with intensities at 70 %, 80 %, and 90 % of the rMT. The TS was delivered at a 0° orientation at 110 % rMT. ISIs of 0.5 ms and 8 ms were used to assess neuronal refractoriness and ICF, respectively. E-field: electric field, CS: conditioning stimulus, rMT: resting motor threshold, TS: test stimulus, ISI: interstimulus interval, ICF: intracortical facilitation. (For interpretation of the references to colour in this figure legend, the reader is referred to the web version of this article.)

43.8, 30.0, and 32.5 μs, while the TS phases were 75.1, 30.0, and 52.7 μs. The resulting mTMS current pulses and E-field waveforms are depicted in Fig. 3.

2.3. Data analysis

We extracted MEPs from the continuous EMG recordings by dividing the signal into epochs from −1 s (pre) to 1 s (post) relative to the TMS pulse. We excluded trials exhibiting muscle pre-activation greater than ± 15 μV within 200 ms before the TMS pulse. About 2.4 % of the epochs were rejected. For each trial, we computed the MEP peak-to-peak amplitude at 15–60 ms after the TMS pulse. We analyzed the data using custom scripts written in MATLAB R2022b (MathWorks, Inc., USA).

We computed a muscle activation map from the HDsEMG grid over the forearm flexor muscles by computing the median of the MEP amplitude across trials for each channel. We determined the MEP amplitude of the activation map as the mean amplitude across the electrodes having at least 70 % of the maximum MEP amplitude based on the watershed algorithm (Souza et al., 2018b, Vieira et al., 2010). Similarly, for each activation map, we calculated the centroid of the segmented channels. The centroid was defined by its x and y coordinates, corresponding to the lateral-medial and proximal–distal axes, respectively, with the most lateral-proximal electrode designated as the origin (0, 0). To assess the spatial specificity of HDsEMG-based MEPs, we compared full-grid HDsEMG quantification with a virtual single electrode positioned over the FCR area for hotspot determination, defined as the signal average across four grid electrodes located at rows 2–3 and columns 3–4 ($x = 3.5$ cm, $y = 2.5$ cm; Supplementary Fig. 3), following previous approaches that derived virtual EMG channels from HDsEMG grids to mimic conventional surface electrodes (Piitulainen et al., 2015; Staudenmann et al., 2006).

We analyzed the effects of CS orientation and intensity, and ISI on MEP amplitudes over the flexor muscles and the corresponding lateral-medial and proximal–distal centroid coordinates, and EDC amplitudes using linear mixed-effects models (Bates et al., 2015; Souza et al., 2025). MEP amplitudes were log-transformed to address unequal variance and positive skewness as deviations from normality (Nielsen, 1996). Data were analyzed with fully crossed fixed effects and random effects nested within subjects. The fixed effects of the model were ISI, CS orientation and intensity, and all interactions between them. The random effects included a random intercept and slopes for ISI, CS orientation, and intensity. The mixed-effects model equations for the logarithm of mean MEP amplitude across the electrodes having at least 70 % of the maximum MEP of the flexor muscles grid, their corresponding lateral-medial and proximal–distal centroid coordinates, and the median MEP amplitudes from the EDC muscle are shown in the Supplementary Table 2. The mixed-effects model equations for comparing log-transformed MEP amplitudes and centroid distances between the HDsEMG grid and the virtual single electrode are also provided in Supplementary Table 2.

To quantify facilitation and suppression, a separate linear mixed-effects model was utilized, comparing all paired-pulse mTMS conditions to the MEPs elicited by the TS alone (single pulse). In this model, the various levels of paired-pulse mTMS (CS orientation and ISI) were grouped to maintain a balanced design, as previously done by Souza et al. (2025). The random effects' structure included only the subject identifiers to account for individual differences in MEP amplitude and centroid coordinate intercepts. Subsequently, we computed F- and p-values for the selected model using a Type-III analysis of variance with Satterthwaite's method. The post-hoc multiple comparisons were computed with estimated marginal means and corrected p-values for false discovery rate (Benjamini and Yekutieli, 2001). We performed model diagnostics with Q–Q plots of residuals to check for deviations from the normal distribution and standard versus fitted values plots to assess heteroscedasticity. The threshold for statistical significance was set at 0.05. The statistical analysis was conducted using custom-written scripts in R 4.4 (R Core Team, 2023) using the *lmer 1.1.35* and *afex 1.3.1* packages for linear mixed-effects models and *emmeans 1.10.2* for computing the estimated marginal means.

3. Results

3.1. Flexor muscles activation

As shown in Table 1, ISI, CS orientation, and intensity significantly affected MEP amplitudes recorded from the forearm flexor muscles. With a 0.5-ms ISI and a CS orientation of 0°, MEPs were suppressed by approximately 90 %, 89 %, and 81 % of the TS alone amplitude for CS intensities at 70 %, 80 %, and 90 % of rMT, respectively. Rotating the CS to 90° (E-field along the central sulcus) yielded reduced suppression of MEP amplitudes by 16 %, 38 %, and 41 % of the TS alone amplitude for CS intensities at 70 %, 80 %, and 90 % of rMT, respectively.

With an 8-ms ISI and a CS intensity of 70 % rMT, the MEP amplitude did not differ from the TS alone for either CS orientation. With an 8-ms ISI and a CS orientation of 0°, MEPs were facilitated by 33 % and 69 % of the TS alone amplitude for CS intensities of 80 % and 90 % of rMT, respectively. Rotating the CS to 90° reduced MEP facilitation by 30 %

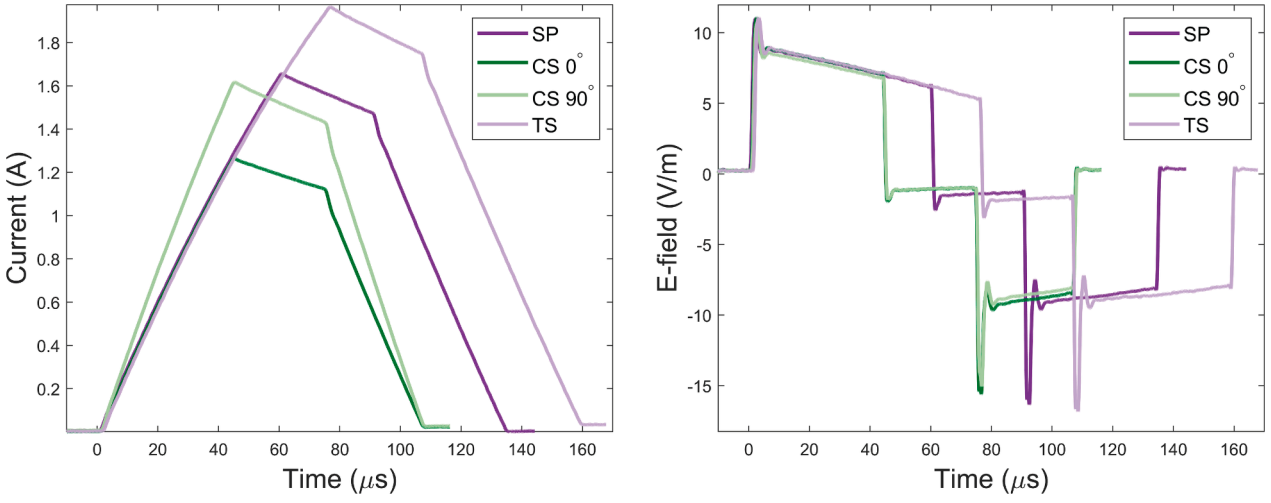


Fig. 3. The mTMS current waveforms on the left and the mTMS E-field waveforms on the right. All waveforms are low-pass filtered at 1 MHz. SP: single pulse, CS: conditioning stimulus, TS: test stimulus.

Table 1
Type III analysis of variance table with Satterthwaite's method for the linear mixed-effects models of MEP amplitudes across the electrode grid.

Effect	Degrees of freedom (num, den)	*F*-value	*p*-value
ISI	(1, 11.0)	130.4	<0.001*
CSO	(1, 11.0)	43.0	<0.001*
CSI	(2, 10.9)	15.5	<0.001*
ISI × CSO	(1, 2744.0)	2930.6	<0.001*
ISI × CSI	(2, 2744.1)	58.0	<0.001*
CSO × CSI	(2, 2744.3)	150.5	<0.001*
ISI × CSO × CSI	(2, 2744.1)	27.1	<0.001*

Note: Interaction between factors is represented as "×". The asterisk (*) indicates statistical significance ($p < 0.05$). ISI: interstimulus interval, CSO: conditioning stimulus orientation, CSI: conditioning stimulus intensity.

Table 2
Type III analysis of variance table with Satterthwaite's method for the linear mixed-effects models of EDC muscle amplitude.

Effect	Degrees of freedom (num, den)	*F*-value	*p*-value
ISI	(1, 11.01)	85.7	<0.001*
CSO	(1, 11.02)	26.6	<0.001*
CSI	(2, 11.09)	10.9	0.002*
ISI × CSO	(1, 2744.65)	932.0	<0.001*
ISI × CSI	(2, 2744.71)	2.9	0.056
CSO × CSI	(2, 2745.24)	57.7	<0.001*
ISI × CSO × CSI	(2, 2744.71)	45.3	<0.001*

Note: Interaction between factors is represented as "×". The asterisk (*) indicates statistical significance ($p < 0.05$). ISI: interstimulus interval, CSO: conditioning stimulus orientation, CSI: conditioning stimulus intensity.

and 18 % of the TS alone for CS intensities of 80 % and 90 % of rMT, respectively.

Facilitation was still prevalent but reduced for CS orientation of 90° (Fig. 4A). The multiple comparisons results for the MEP amplitude of the flexor muscles are given in Supplementary Table 3. Subject-specific MEP amplitude patterns across all stimulation conditions are shown in Supplementary Fig. 1.

3.2. Extensor muscle activation

Table 2 indicates a significant interaction between ISI, CS orientation, and intensity on the MEP amplitude from the EDC muscle. As illustrated in Fig. 4B, with 0.5-ms ISI and CS orientation 0°, MEPs were suppressed by approximately 95 %, 96 %, and 84 % of the TS alone amplitude at CS intensities of 70 %, 80 %, and 90 % rMT, respectively. Changing the CS orientation to 90° yielded substantially reduced MEP suppression by 48 %, 45 %, and 61 % of the TS alone amplitude for CS intensities of 70 %, 80 %, and 90 % rMT, respectively.

With an 8-ms ISI and a CS orientation of 0°, the EDC amplitude increased by 13 %, 48 %, and 86 % relative to the TS alone amplitude for CS intensities of 70 %, 80 % and 90 %, respectively. Switching to a 90° CS orientation lowered this enhancement, resulting in EDC MEP amplitude facilitation by 1 %, 3 %, and 32 % of the TS alone at CS intensities of 70 %, 80 % and 90 %, respectively. The multiple comparisons results for the MEP amplitude of the ECR muscle are given in Supplementary Table 4. Subject-specific EDC amplitude responses for each condition are presented in Supplementary Fig. 1.

3.3. Spatial shifts in the centroid of activation maps

Table 3 demonstrates that the interactions between CS intensity and orientation, as well as CS orientation and ISI, were significant on the centroid location along the lateral-medial axis. As illustrated in Fig. 5, with 0.5-ms ISI, the centroid shifted laterally across all CS orientation and intensity conditions. Specifically, for CS orientation 0°, the centroid shifted laterally by 2.7 and 2.2 mm relative to the TS alone at CS intensities of 70 % and 80 %, respectively. At a CS intensity of 90 %, there was almost the same spatial activation pattern in the lateral-medial direction. For CS orientation 90°, the centroid had lateral shifts of 1.1 and 2.2 mm for CS intensities of 70 % and 90 %, respectively, whereas at a CS intensity of 80 %, there was almost the same spatial activation pattern in the lateral-medial direction.

Table 3
Type III analysis of variance table with Satterthwaite's method for the linear mixed-effects models of the centroid on the lateral–medial axis.

Effect	Degrees of freedom (num, den)	*F*-value	*p*-value
ISI	(1, 11.0)	14.4	0.003
CSO	(1, 11.0)	0.4	0.53
CSI	(2, 2727.3)	4.3	0.014*
ISI × CSO	(1, 2731.9)	4.8	0.028*
ISI × CSI	(2, 2727.4)	1.7	0.18
CSO × CSI	(2, 2727.3)	4.2	0.015*
ISI × CSO × CSI	(2, 2727.3)	0.06	0.933

Note: Interaction between factors is represented as "×". The asterisk (*) indicates statistical significance ($p < 0.05$). ISI: interstimulus interval, CSO: conditioning stimulus orientation, CSI: conditioning stimulus intensity.

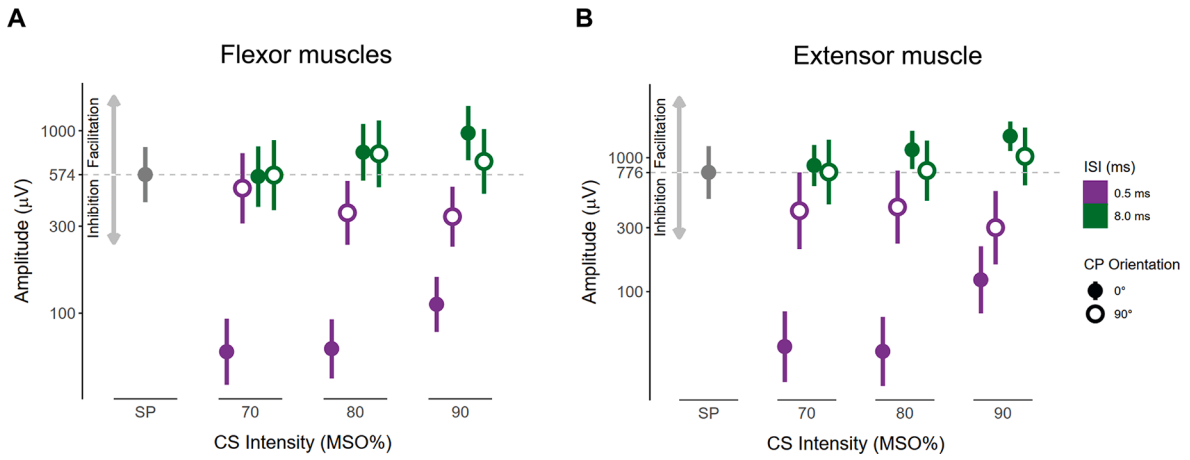


Fig. 4. Linear mixed-effects model results for flexor and extensor muscle activation amplitudes. A) Effects of CS orientation, CS intensity, and ISI on the monopolar MEP amplitude as the average of the segmented channels of the HDsEMG grid over the forearm flexor muscles. B) Effects of CS orientation, CS intensity, and ISI on MEP amplitude of the extensor digitorum communis muscle. SP: single pulse, CS: conditioning stimulus, ISI: interstimulus interval, MSO: maximum stimulator output.

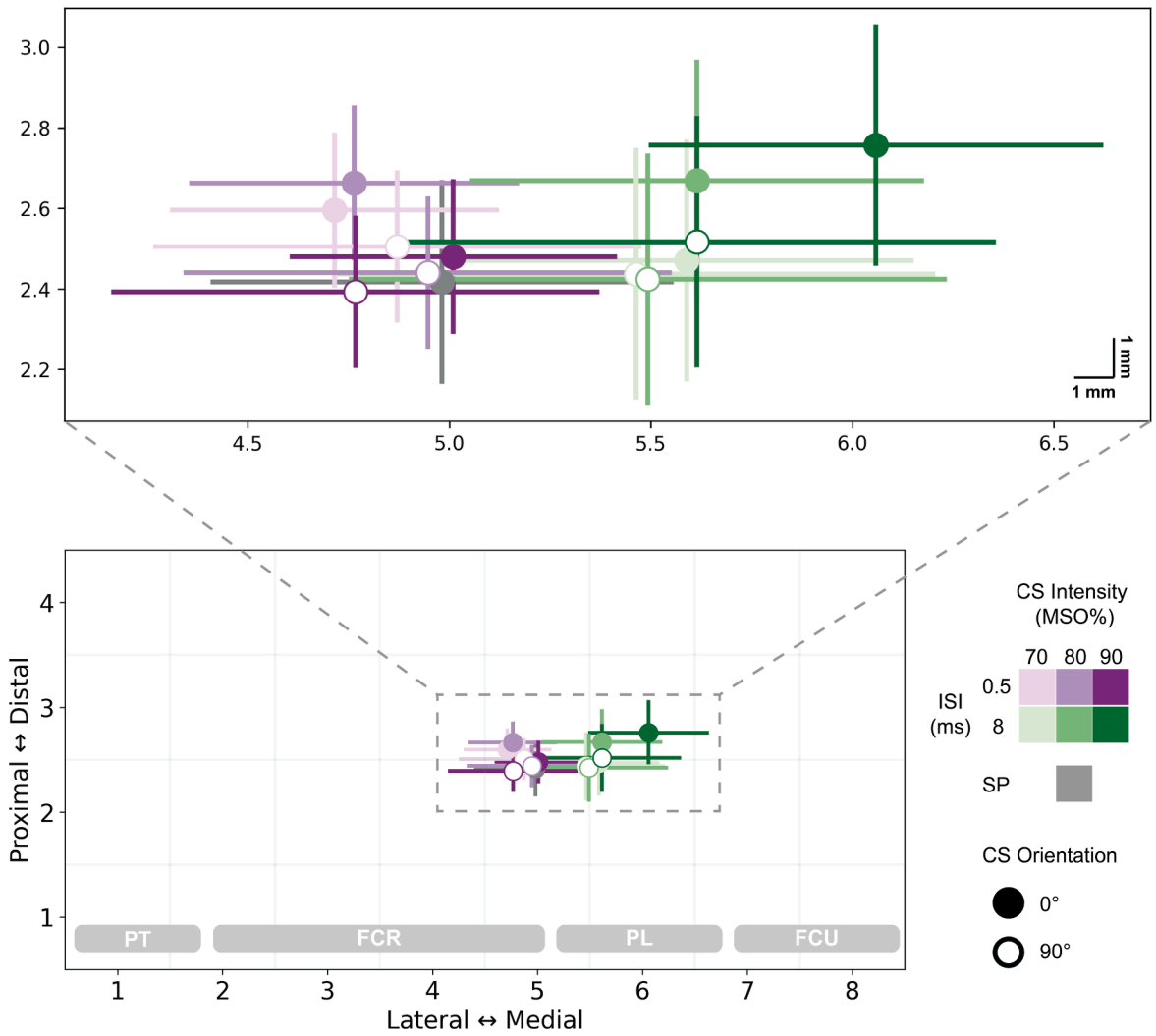


Fig. 5. Effect of CS orientation, CS intensity, and ISI on centroid coordinates of the MEP activation map on the lateral-medial and the proximal–distal directions. The approximate locations of the superficial flexor muscles are shown at the bottom of the grid. SP: single pulse, CS: conditioning stimulus, ISI: interstimulus interval, MSO: maximum stimulator output, PT: pronator teres, FCR: flexor carpi radialis, PL: palmaris longus, FCU: flexor carpi ulnaris.

With an 8-ms ISI, the centroid shifted medially for all CS orientations and intensity conditions. For both orientations, the medial shift increased with CS intensity. Specifically, for CS orientation 0°, the centroid differed from the TS alone by 6.1, 6.3, and 10.8 mm at CS intensities of 70 %, 80 %, and 90 %, respectively. For CS orientation 90°, the centroid shifted by 4.8, 5.1, and 6.3 mm medially for CS intensities of 70 %, 80 %, and 90 %, respectively. The multiple comparisons results for the centroid location in the lateral-medial axis are given in Supplementary Table 5.

Table 4
Type III analysis of variance table with Satterthwaite's method for the linear mixed-effects models of the centroid on the proximal–distal axis.

Effect	Degrees of freedom (num, den)	*F*-value	*p*-value
ISI	(1, 11.0)	0.11	0.75
CSO	(1, 11.1)	9.7	0.009*
CSI	(2, 2655.4)	1.6	0.2
ISI × CSO	(1, 2656)	0.77	0.38
ISI × CSI	(2, 2655.8)	15.7	<0.001*
CSO × CSI	(2, 2655.7)	5.1	0.006*
ISI × CSO × CSI	(2, 2655.4)	1.9	0.147

Note: Interaction between factors is represented as "×". The asterisk (*) indicates statistical significance ($p < 0.05$). ISI: interstimulus interval, CSO: conditioning stimulus orientation, CSI: conditioning stimulus intensity.

Table 4 demonstrates that the CS orientation and its interaction with CS intensity significantly influenced the centroid position along the proximal–distal axis. Moreover, the interaction between CS intensity and ISI had a highly significant effect, suggesting these factors interactively impacted the centroid position. In all conditions, the centroid shifted distally in comparison with the TS alone, except for ISI 0.5 ms and CS orientation of 90° at CS intensity of 90 % which was almost the same as the TS alone. Specifically, with ISI 0.5 ms and for CS orientation of 0°, the centroid shifted distally by 1.8 and 2.5 mm for CS intensities of 70 % and 80 %, respectively. With ISI 8 ms and for CS orientation 0°, the centroid shifted distally by 2.5 and 3.4 mm for CS intensities of 80 % and 90 %, respectively. By changing the orientation to 90°, the centroid shifted 1 mm distally for the CS intensity of 90 %. The multiple comparisons results for the centroid location in the proximal–distal axis are given in Supplementary Table 6. In addition, centroid shifts for individual subjects across all stimulation conditions are shown in Supplementary Fig. 2.

3.4. Comparison between HDsEMG and virtual single-electrode MEPs

The MEP amplitude significantly differed between electrode types, with HDsEMG yielding higher MEP amplitudes than the virtual electrode ($F(1,11) = 29.71, p < 0.001$). Significant electrode type × ISI × CS-

intensity interactions on the linear mixed-effects model indicated that the MEP amplitude recorded with the HDsEMG grid and the virtual single electrode varied across paired-pulse parameters (Supplementary Table 7). The multiple comparisons for the MEP amplitudes obtained from the HDsEMG grid and the virtual single electrode are presented in Supplementary Table 8.

The centroid of HDsEMG activation also varied with stimulation parameters. A linear mixed-effects model demonstrated significant main effects of ISI ($F(1,2788) = 87.9$, $p < 0.001$) and CS intensity ($F(2,2788) = 4.02$, $p = 0.018$), as well as a significant ISI × CS-orientation interaction ($F(1,2788) = 13.61$, $p < 0.001$; Supplementary Table 9). These results show that the spatial locus of maximal muscle activation shifts systematically with paired-pulse parameters. The multiple comparisons for the centroid distances between HDsEMG and the virtual electrode position are reported in Supplementary Table 10.

4. Discussion

In this study, we investigated the effects of CS orientation, ISI, and CS intensity on the facilitation and suppression of forearm muscle spatial activation using paired-pulse TMS with a high-precision mTMS system and HDsEMG. Our findings demonstrate that stimulus orientation significantly affects the motor cortex facilitation and inhibition, as evidenced by the corticospinal MEPs in the superficial wrist flexor muscles (FCR, PL, and FCU), and that both the amplitude and spatial distribution of MEPs are shaped by the interaction between ISI, CS intensity, and current direction.

4.1. Cortical excitability modulated by stimulation conditions

Our results showed that a 0.5-ms ISI induces significant suppression of MEP amplitude, particularly when the CS orientation is 0° (anterior-to-medial), consistent with prior evidence attributing short-interval suppression to neuronal refractoriness (Fisher et al., 2002; Hanajima et al., 1998; Roshan et al., 2003; Souza et al., 2025). The reduced suppression observed when the CS orientation was changed to 90° (along the central sulcus), from MEP amplitudes of ~10 % to ~84 % of the TS alone response at 70 % rMT, confirms that E-field direction plays a critical role in recruiting overlapping cortical populations into refractory states. This spatial selectivity aligns with findings from Souza et al. (2025), where orientation-specific neuronal refractoriness was also observed in intrinsic hand muscles. These results support the view that probing neuronal refractoriness is both time- and direction-dependent, influenced by the alignment between the E-field and the orientation of affected cortical neurons (Chen et al., 2003; Ziemann et al., 1996).

In contrast, the 8-ms ISI condition predominantly led to facilitation of MEPs, in line with the recruitment of intracortical excitatory circuits associated with ICF (Chen, 2004; Ziemann et al., 1998b). Facilitation was most prominent at 90 % rMT and with the CS oriented at 0°, resulting in a ~69 % increase relative to the TS alone amplitude. At 70 % rMT, no facilitation was observed, indicating that a minimum excitability threshold is needed to recruit facilitatory circuits. These findings highlight that facilitation is both orientation-specific and intensity-sensitive, likely reflecting the recruitment thresholds of distinct cortical interneuron pools (Säisänen et al., 2011; Tugin et al., 2021; Volz et al., 2015).

The relatively low TS intensity (110 % rMT) may have increased response variability across subjects (Brown et al., 2017; Goetz et al., 2014; Spampinato et al., 2023). However, this TS intensity was selected to ensure more focal cortical activation (Tardelli et al., 2022; van de Ruit and Grey, 2016) and to enhance orientation-sensitivity of cortical circuits (i.e., sharper dependence of MEP amplitude on stimulus orientation) (Kallioniemi et al., 2015; Souza et al., 2022; Souza et al., 2025; Weise et al., 2023).

Because the 110 % rMT TS intensity produced smaller baseline MEPs in some participants (see Supplementary Fig. 1), floor effects, particularly at CS orientation 0°, may have led to an underestimation of the difference between CS orientation 0° and CS orientation 90° conditions. Future studies employing higher TS intensities could clarify whether the observed effects differ in magnitude under these conditions.

4.2. Spatial organization of muscle activation

The HDsEMG revealed how stimulation conditions affect the spatial topography of muscle activation, i.e., how different motor units of the superficial wrist flexors were activated on average in each studied condition. With 0.5-ms ISI, the MEP activation centroid consistently shifted laterally, particularly with CS orientation of 0°, suggesting that the primary target muscle, FCR, was inhibited more than the more lateral muscles. This may reflect neuronal refractoriness and compensatory recruitment of adjacent cortical areas. The lateral shift reached up to 2.7 mm depending on CS intensity and orientation. This finding is consistent with previous work showing orientation-dependent recruitment of distributed cortical subpopulations (Fong et al., 2021; Souza et al., 2025).

With 8-ms ISI, the centroid shifted medially across all CS intensities and orientations, with larger shifts occurring at higher intensities. For example, with 90 % rMT and 0° orientation, the shift reached ~10.8 mm. These changes suggest enhanced recruitment of cortical facilitatory neuronal networks specifically targeting the FCR, our primary target muscle. This indicates that, like inhibition, facilitation may also be spatially focused toward the primary motor representations, i.e., muscles' somatotopic representations. This is consistent with the connectivity-dependent facilitation observed in earlier studies (Volz et al., 2015).

Interestingly, the centroid of activation was slightly shifted from the estimated innervation zone, which was originally identified based on an atlas of muscle innervation zones (Barbero et al., 2012). This highlights a key advantage of HDsEMG, as it captures the spatial distribution of muscle activity more comprehensively than a single channel, despite the latter's relatively large detection volume potentially being sufficient in some cases.

Across both ISIs, the centroid also shifted distally relative to the TS alone, particularly with higher intensities and 0° CS orientation. These distal shifts suggest spatial reorganization of motor output, potentially reflecting the recruitment of alternate descending pathways or broader cortical regions at higher excitability levels.

The directional effects of CS orientation on spatial shifts were not strictly bidirectional as initially interpreted. Rather than a clear medial vs. lateral shift dependent on ISI and orientation, the shifts were generally lateral for 0.5-ms ISI and medial for 8-ms ISI, regardless of CS orientation. The medio-lateral emphasis in spatial muscle activation can be explained by anatomical considerations. The HDsEMG grid partially covered three superficial muscles, making it likely that changes in cortically recruited corticospinal neurons differentially activated the medial or lateral compartment of the flexor muscle group. The CS orientation effect was more pronounced in modulating the magnitude of shifts rather than reversing their direction. This suggests that ISI may have a stronger influence on spatial recruitment patterns than orientation alone. Previous studies using HDsEMG have shown that TMS-evoked motor responses in the forearm muscles diverge spatially from those seen during voluntary contractions, particularly as stimulus intensity increases (van Elswijk et al., 2008). In line with this, our results show that paired-pulse stimulation induces distinct shifts in the spatial activation of forearm flexors, extending these findings by revealing orientation- and timing-specific reorganization patterns at high spatial resolution.

4.3. Methodological considerations and clinical implications

While most paired-pulse TMS studies have focused on intrinsic hand muscles (Kujirai et al., 1993; Ziemann et al., 1996), our results

demonstrate that orientation- and ISI-dependent effects apply to forearm flexors, though with distinct spatial patterns. It is important to note that the relatively small differences in spatial distribution across conditions may partly reflect anatomical variability within subjects, such as differences in forearm size. In our statistical analysis, we accounted for such variability by using a linear mixed-effects model with subjects as a random factor. Alternatively, spatial differences could be normalized to specific forearm measurements, such as circumference or length, to enable more accurate comparisons across subjects in future studies. Nonetheless, the clear orientation dependence of both amplitude and spatial features reinforces the importance of precise E-field control in TMS studies.

HDsEMG provides a spatially resolved measure of TMS-evoked muscle activity, reducing ambiguity caused by volume conduction and crosstalk inherent to single-channel surface EMG. In conventional EMG, the recorded signal reflects a spatially weighted sum of motor-unit territories and adjacent muscles, so shifts in the spatial distribution of recruited units can change single-channel MEP amplitude independently of corticospinal drive (Farina et al., 2004; van Elswijk et al., 2008). Accordingly, a fixed electrode may underestimate facilitation when activation shifts away from it or underestimate inhibition when activation shifts toward it.

In this study, HDsEMG consistently detected larger MEP amplitudes than a virtual single electrode, and the magnitude of this difference varied with ISI and stimulus intensity, indicating that spatial shifts in muscle activation contribute to condition-dependent modulation patterns. Centroid displacements reached ~10 mm, which is not negligible for forearm flexors, where multiple superficial muscles overlap within a few centimeters (Campanini et al., 2022). These shifts likely reflect condition-dependent variations in motor-unit recruitment rather than large-scale cortical reorganization (Skarabot et al., 2023). Together, these results demonstrate that HDsEMG offers topographical information about how facilitation and inhibition appear at the muscular level, which cannot be obtained from a single surface electrode.

Importantly, such spatial shifts are not negligible in a clinical context. Paired-pulse TMS paradigms such as SICI and ICF are increasingly used to probe intracortical inhibitory and excitatory mechanisms in neurological disorders, including amyotrophic lateral sclerosis, Parkinson's disease, and neuropathic pain (Kindred et al., 2024; Tankisi et al., 2025; Vucic et al., 2023). Since clinical protocols typically rely on a single bipolar or monopolar electrode (belly-tendon montage) (Garcia et al., 2017; Rossini et al., 2015), spatial displacement of muscle activation can mimic changes in intracortical excitability and affect diagnostic interpretation. These outcomes underscore the need for precise electrode placement and careful interpretation when paired-pulse TMS is applied to forearm muscles and support the use of spatially informed EMG approaches to improve the reliability of excitability assessments (Souza et al., 2018; van Elswijk et al., 2008).

Moreover, these findings can have clinical relevance for neurorehabilitation. For instance, after a stroke, cortical excitability and somatotopic organization are often disrupted, leading to impaired motor control and altered muscle recruitment patterns (Traversa et al., 1997). The orientation- and intensity-specific facilitation and suppression effects observed here suggest that individualized, directionally-targeted TMS protocols could be developed to selectively engage preserved cortical pathways or reorganize disrupted networks. Additionally, the use of HDsEMG to capture spatial aspects of muscle activation could aid in tracking recovery or guiding therapy by identifying changes in motor unit recruitment and mapping responses over time (Miller et al., 2019). Future research should explore whether these findings generalize to motor learning paradigms or patient populations with disrupted excitability and cortical organization, such as stroke survivors.

5. Conclusion

This study highlights the feasibility and value of combining mTMS with HDsEMG to resolve the spatial and temporal dynamics of corticomotor output in superficial forearm flexors under paired-pulse TMS protocols. We show that short ISIs (0.5 ms) produce robust MEP suppression via orientation-dependent neuronal refractoriness, while longer intervals (8 ms) elicit facilitation through intracortical excitatory mechanisms. Both the amplitude and spatial distribution of MEPs were systematically modulated by CS orientation and intensity, with mTMS enabling precise and repeatable control of E-field direction. These findings reveal that stimulation conditions shape not only the strength but also the spatial pattern of muscle activations, providing new insights into the directional and intensity tuning of forearm motor representations. This has implications for improving the neurophysiological specificity and efficacy of TMS-based neuromodulation strategies targeting upper limb function.

Data statement

The data that support the findings of this study are available from the corresponding author upon reasonable request. Detailed statistical analyses, including multiple comparisons results and subject-specific data, are provided in the Supplementary Material.

CRediT authorship contribution statement

Shokoofeh Parvin: Conceptualization, Methodology, Software, Formal analysis, Investigation, Data curation, Writing – original draft, Writing – review & editing, Visualization, Funding acquisition. **Joona Juurakko:** Conceptualization, Methodology, Software, Investigation, Writing – review & editing. **Heikki Sinisalo:** Validation, Resources, Writing – review & editing. **Giacinto L. Cerone:** Software, Validation, Resources, Writing – review & editing. **Alberto Botter:** Software, Validation, Resources, Writing – review & editing. **Risto J. Ilmoniemi:** Resources, Writing – review & editing, Funding acquisition. **Harri Piitulainen:** Conceptualization, Methodology, Software, Writing – review & editing, Supervision, Funding acquisition. **Victor H. Souza:** Conceptualization, Methodology, Software, Investigation, Writing – original draft, Writing – review & editing, Visualization, Supervision, Funding acquisition.

Declaration of competing interest

The authors declare the following financial interests/personal relationships which may be considered as potential competing interests: H.S., R.J.I., and V.H.S. are inventors of patents for TMS technology and founders of Cortisys Inc. R.J.I. and V.H.S. have received unrelated consulting fees from Nexstim Plc. The other authors declare no conflict of interest.

Acknowledgments

This work was supported by Jenny and Antti Wihuri Foundation, Ella and Georg Ehrnrooth Foundation, KAUTE Foundation, Finnish Foundation for Technology Promotion, European Research Council (ERC Synergy) under the European Union's Horizon 2020 (ConnectToBrain; grant No 810377), and Research Council of Finland (Decisions No. 349985 and 361732). We acknowledge the computational resources provided by the Aalto Science-IT.

Appendix A. Supplementary data

Supplementary data to this article can be found online at https://doi.org/10.1016/j.clinph.2025.2111477.

References

Awiszus, F., 2003. TMS and threshold hunting. Suppl. Clin. Neurophysiol. 56, 13–23. https://doi.org/10.1016/s1567-424x(09)70205-3.

Barbero M, Merletti R, Rainoldi A. Atlas of Muscle Innervation Zones. 2012.

Barker, A.T., Garnham, C.W., Freeston, I.L., 1991. Magnetic nerve stimulation: the effect of waveform on efficiency, determination of neural membrane time constants and the measurement of stimulator output. Electroencephalogr. Clin. Neurophysiol. Suppl. 43, 227–237.

Barker, A.T., Jalinous, R., Freeston, I.L., 1985. Non-invasive magnetic stimulation of human motor cortex. Lancet 1 (8437), 1106–1107. https://doi.org/10.1016/s0140-6736(85)92413-4.

Bashir, S., Perez, J.M., Horvath, J.C., Pascual-Leone, A., 2013. Differentiation of motor cortical representation of hand muscles by navigated mapping of optimal TMS current directions in healthy subjects. J. Clin. Neurophysiol. 30 (4), 390–395. https://doi.org/10.1097/WNP.0b013e31829dda6b.

Bates, D., Mächler, M., Bolker, B., Walker, S., 2015. Fitting linear mixed-effects models using lme4. J. Stat. Softw. 67 (1), 10.18637/jss.v067.i01.

Benjamini, Y., Yekutieli, D., 2001. The control of the false discovery rate in multiple testing under dependency. Ann. Stat. 29 (4), 1165–1188. https://doi.org/10.1214/aos/1013699998.

Brown, K.E., Lohse, K.R., Mayer, I.M.S., Strigaro, G., Desikan, M., Casula, E.P., et al., 2017. The reliability of commonly used electrophysiology measures. Brain Stimul. 10 (6), 1102–1111. https://doi.org/10.1016/j.brs.2017.07.011.

Campanini, I., Merlo, A., Disselhorst-Klug, C., Mesin, L., Muceli, S., Merletti, R., 2022. Fundamental concepts of bipolar and high-density surface EMG understanding and teaching for clinical, occupational and sport applications: origin, detection, and main errors. Sensors (Basel) 22. https://doi.org/10.3390/s22114150.

Cerone, G.L., Botter, A., Gazzoni, M., 2019. A modular, smart, and wearable system for high density sEMG detection. I.E.E.E. Trans. Biomed. Eng. 66 (12), 3371–3380. https://doi.org/10.1109/TBME.2019.2904398.

Cerone, G.L., Giangrande, A., Ghislieri, M., Gazzoni, M., Piitulainen, H., Botter, A., 2022. Design and validation of a wireless body sensor network for integrated EEG and HD-sEMG acquisitions. IEEE Trans. Neural Syst. Rehabil. Eng. 30, 61–71. https://doi.org/10.1109/TNSRE.2022.3140220.

Chen, R., 2004. Interactions between inhibitory and excitatory circuits in the human motor cortex. Exp. Brain Res. 154 (1), 1–10. https://doi.org/10.1007/s00221-003-1684-1.

Chen, R., Yung, D., Li, J.-Y., 2003. Organization of ipsilateral excitatory and inhibitory pathways in the human motor Cortex. J. Neurophysiol. 89 (3), 1256–1264. https://doi.org/10.1152/jn.00950.2002.

Chen, R., Tam, A., Butefisch, C., Corwell, B., Ziemann, U., Rothwell, J.C., et al., 1998. Intracortical inhibition and facilitation in different representations of the human motor cortex. J. Neurophysiol. 80 (6), 2870–2881. https://doi.org/10.1152/jn.1998.80.6.2870.

D'Ostilio, K., Goetz, S.M., Hannah, R., Ciocca, M., Chieffo, R., Chen, J.A., et al., 2016. Effect of coil orientation on strength-duration time constant and I-wave activation with controllable pulse parameter transcranial magnetic stimulation. Clin. Neurophysiol. 127 (1), 675–683. https://doi.org/10.1016/j.clinph.2015.05.017.

Davey, N.J., Smith, H.C., Savic, G., Maskill, D.W., Ellaway, P.H., Frankel, H.L., 1999. Comparison of input-output patterns in the corticospinal system of normal subjects and incomplete spinal cord injured patients. Exp. Brain Res. 127 (4), 382–390. https://doi.org/10.1007/s002210050806.

Del Vecchio, A., Casolo, A., Negro, F., Scorcelletti, M., Bazzucchi, I., Enoka, R., et al., 2019. The increase in muscle force after 4 weeks of strength training is mediated by adaptations in motor unit recruitment and rate coding. J. Physiol. 597 (7), 1873–1887. https://doi.org/10.1113/JP277250.

Di Lazzaro, V., Oliviero, A., Mazzone, P., Insola, A., Pilato, F., Saturno, E., et al., 2001. Comparison of descending volleys evoked by monophasic and biphasic magnetic stimulation of the motor cortex in conscious humans. Exp. Brain Res. 141 (1), 121–127. https://doi.org/10.1007/s002210100863.

Farina, D., Merletti, R., Enoka, R.M., 2004. The extraction of neural strategies from the surface EMG. J. Appl. Physiol. (1985) 96 (4), 1486–1495. https://doi.org/10.1152/japplphysiol.01070.2003.

Fisher, R.J., Nakamura, Y., Bestmann, S., Rothwell, J.C., Bostock, H., 2002. Two phases of intracortical inhibition revealed by transcranial magnetic threshold tracking. Exp. Brain Res. 143 (2), 240–248. https://doi.org/10.1007/s00221-001-0988-2.

Fong, P.Y., Spampinato, D., Rocchi, L., Hannah, R., Teng, Y., Di Santo, A., et al., 2021. Two forms of short-interval intracortical inhibition in human motor cortex. Brain Stimul. 14 (5), 1340–1352. https://doi.org/10.1016/j.brs.2021.08.022.

Fox, P.T., Narayana, S., Tandon, N., Sandoval, H., Fox, S.P., Kochunov, P., et al., 2004. Column-based model of electric field excitation of cerebral cortex. Hum. Brain Mapp. 22 (1), 1–14. https://doi.org/10.1002/hbm.20006.

Gallina, A., Botter, A., 2013. Spatial localization of electromyographic amplitude distributions associated to the activation of dorsal forearm muscles. Front. Physiol. 4, 367. https://doi.org/10.3389/fphys.2013.00367.

Garcia, M.A.C., Souza, V.H., Vargas, C.D., 2017. Can the recording of motor potentials evoked by transcranial magnetic stimulation be optimized? Front. Hum. Neurosci. 11, 413. https://doi.org/10.3389/fnhum.2017.00413.

Goetz, S.M., Luber, B., Lisanby, S.H., Peterchev, A.V., 2014. A novel model incorporating two variability sources for describing motor evoked potentials. Brain Stimul. 7 (4), 541–552. https://doi.org/10.1016/j.brs.2014.03.002.

Gomez-Tames, J., Hamasaka, A., Laakso, I., Hirata, A., Ugawa, Y., 2018. Atlas of optimal coil orientation and position for TMS: a computational study. Brain Stimul. 11 (4), 839–848. https://doi.org/10.1016/j.brs.2018.04.011.

Hamada, M., Murase, N., Hasan, A., Balaratnam, M., Rothwell, J.C., 2013. The role of interneuron networks in driving human motor cortical plasticity. Cereb. Cortex 23 (7), 1593–1605. https://doi.org/10.1093/cercor/bhs147.

Hanajima, R., Ugawa, Y., Terao, Y., Sakai, K., Furubayashi, T., Machii, K., et al., 1998. Paired-pulse magnetic stimulation of the human motor cortex: differences among I waves. J. Physiol. 509 (2), 607–618. https://doi.org/10.1111/j.1469-7793.1998.607bn.x.

Hess, C.W., Mills, K.R., Murray, N.M., Schriefer, T.N., 1987. Magnetic brain stimulation: central motor conduction studies in multiple sclerosis. Ann. Neurol. 22 (6), 744–752. https://doi.org/10.1002/ana.410220611.

Jiang, N., Wang, L., Huang, Z., Li, G., 2021. Mapping responses of lumbar paravertebral muscles to single-pulse cortical TMS using high-density surface electromyography. IEEE Trans. Neural Syst. Rehabil. Eng. 29, 831–840. https://doi.org/10.1109/TNSRE.2021.3076095.

Kallioniemi, E., Könönen, M., Julkunen, P., 2015. Repeatability of functional anisotropy in navigated transcranial magnetic stimulation–coil-orientation versus response. Neuroreport 26 (9), 515–521. https://doi.org/10.1097/WNR.0000000000000380.

Kaneko, K., Kawai, S., Fuchigami, Y., Morita, H., Ofuji, A., 1996. The effect of current direction induced by transcranial magnetic stimulation on the corticospinal excitability in human brain. Electroencephalogr. Clin. Neurophysiol./Electromyogr. Motor Contr. 101 (6), 478–482. https://doi.org/10.1016/s0921-884x(96)96021-x.

Kindred, J.H., Gregory, C.M., Kautz, S.A., Bowden, M.G., 2024. Interhemispheric asymmetries in intracortical facilitation correlate with fatigue severity in individuals with poststroke fatigue. J. Clin. Neurophysiol. 41 (4), 365–372. https://doi.org/10.1097/WNP.0000000000000994.

Koponen, L.M., Nieminen, J.O., Mutanen, T.P., Ilmoniemi, R.J., 2018. Noninvasive extraction of microsecond-scale dynamics from human motor cortex. Hum. Brain Mapp. 39 (6), 2405–2411. https://doi.org/10.1002/hbm.24010.

Kujirai, T., Caramia, M.D., Rothwell, J.C., Day, B.L., Thompson, P.D., Ferbert, A., et al., 1993. Corticocortical inhibition in human motor cortex. J. Physiol. 471, 501–519. https://doi.org/10.1113/jphysiol.1993.sp019912.

Laakso, I., Hirata, A., Ugawa, Y., 2014. Effects of coil orientation on the electric field induced by TMS over the hand motor area. Phys. Med. Biol. 59 (1), 203–218. https://doi.org/10.1088/0031-9155/59/1/203.

Ma, K., Hamada, M., Di Lazzaro, V., Hand, B., Guerra, A., Opie, G.M., et al., 2023. Correlating active and resting motor thresholds for transcranial magnetic stimulation through a matching model. Brain Stimul. 16 (6), 1686–1688. https://doi.org/10.1016/j.brs.2023.11.009.

Merletti, R., Aventaggiato, M., Botter, A., Holobar, A., Marateb, H., Vieira, T.M., 2010. Advances in surface EMG: recent progress in detection and processing techniques. Crit. Rev. Biomed. Eng. 38 (4), 305–345. https://doi.org/10.1615/critrevbiomedeng.v38.i4.10.

Miller, K.J., Gallina, A., Neva, J.L., Ivanova, T.D., Snow, N.J., Ledwell, N.M., et al., 2019. Effect of repetitive transcranial magnetic stimulation combined with robot-assisted training on wrist muscle activation post-stroke. Clin. Neurophysiol. 130 (8), 1271–1279. https://doi.org/10.1016/j.clinph.2019.04.712.

Neva, J.L., Gallina, A., Peters, S., Garland, S.J., Boyd, L.A., 2017. Differentiation of motor evoked potentials elicited from multiple forearm muscles: an investigation with high-density surface electromyography. Brain Res. 1676, 91–99. https://doi.org/10.1016/j.brainres.2017.09.017.

Nielsen, J.F., 1996. Logarithmic distribution of amplitudes of compound muscle action potentials evoked by transcranial magnetic stimulation. J. Clin. Neurophysiol. 13 (5), 423–434. https://doi.org/10.1097/00004691-199609000-00005.

Nieminen, J.O., Koponen, L.M., Mäkelä, N., Souza, V.H., Stenroos, M., Ilmoniemi, R.J., 2019. Short-interval intracortical inhibition in human primary motor cortex: a multi-locus transcranial magnetic stimulation study. Neuroimage 203, 116194. https://doi.org/10.1016/j.neuroimage.2019.116194.

Nikolov, P., Zimmermann, J.V., Hassan, S.S., Albrecht, P., Schnitzler, A., Groiss, S.J., 2021. Impact of the number of conditioning pulses on motor cortex excitability: a transcranial magnetic stimulation study. Exp. Brain Res. 239 (2), 583–589. https://doi.org/10.1007/s00221-020-06010-7.

Oldfield, R.C., 1971. The assessment and analysis of handedness: the Edinburgh inventory. Neuropsychologia 9 (1), 97–113. https://doi.org/10.1016/0028-3932(71)90067-4.

Opitz, A., Legon, W., Rowlands, A., Bickel, W.K., Paulus, W., Tyler, W.J., 2013. Physiological observations validate finite element models for estimating subject-specific electric field distributions induced by transcranial magnetic stimulation of the human motor cortex. Neuroimage 81, 253–264. https://doi.org/10.1016/j.neuroimage.2013.04.067.

Piitulainen, H., Botter, A., Bourguignon, M., Jousmäki, V., Hari, R., 2015. Spatial variability in cortex-muscle coherence investigated with magnetoencephalography and high-density surface electromyography. J. Neurophysiol. 114 (5), 2843–2853. https://doi.org/10.1152/jn.00574.2015.

Roshan, L., Paradiso, G.O., Chen, R., 2003. Two phases of short-interval intracortical inhibition. Exp. Brain Res. 151 (3), 330–337. https://doi.org/10.1007/s00221-003-1502-9.

Rossini, P.M., Burke, D., Chen, R., Cohen, L.G., Daskalakis, Z., Di Iorio, R., et al., 2015. Non-invasive electrical and magnetic stimulation of the brain, spinal cord, roots and peripheral nerves: basic principles and procedures for routine clinical and research application. An updated report from an I.F.C.N. Committee. Clin Neurophysiol. 126 (6), 1071–1107. https://doi.org/10.1016/j.clinph.2015.02.001.

Säisänen, L., Julkunen, P., Niskanen, E., Hukkanen, T., Mervaala, E., Karhu, J., et al., 2011. Short- and intermediate-interval cortical inhibition and facilitation assessed by navigated transcranial magnetic stimulation. J. Neurosci. Methods 195 (2), 241–248. https://doi.org/10.1016/j.jneumeth.2010.11.022.

Schwenkreis, P., Witscher, K., Janssen, F., Addo, A., Dertwinkel, R., Zenz, M., et al., 1999. Influence of the N-methyl-D-aspartate antagonist memantine on human motor cortex excitability. Neurosci. Lett. 270 (3), 137–140. https://doi.org/10.1016/s0304-3940(99)00492-9.

Skarabot, J., Ammann, C., Balshaw, T.G., Divjak, M., Urh, F., Murks, N., et al., 2023. Decoding firings of a large population of human motor units from high-density surface electromyogram in response to transcranial magnetic stimulation. J. Physiol. 601 (10), 1719–1744. https://doi.org/10.1113/JP284043.

Souza, V.H., Baffa, O., Garcia, M.A.C., 2018a. Lateralized asymmetries in distribution of muscular evoked responses: an evidence of specialized motor control over an intrinsic hand muscle. Brain Res. 1684, 60–66. https://doi.org/10.1016/j.brainres.2018.01.031.

Souza, V.H., Nieminen, J.O., Tugin, S., Koponen, L.M., Baffa, O., Ilmoniemi, R.J., 2022. TMS with fast and accurate electronic control: measuring the orientation sensitivity of corticomotor pathways. Brain Stimul. 15 (2), 306–315. https://doi.org/10.1016/j.brs.2022.01.009.

Souza, V.H., Nieminen, J.O., Tugin, S., Koponen, L.M., Ziemann, U., Baffa, O., et al., 2025. Probing the orientation specificity of excitatory and inhibitory circuitries in the primary motor cortex with multi-channel TMS. Clin. Neurophysiol. 169, 23–32. https://doi.org/10.1016/j.clinph.2024.11.004.

Souza, V.H., Vieira, T.M., Peres, A.S.C., Garcia, M.A.C., Vargas, C.D., Baffa, O., 2018b. Effect of TMS coil orientation on the spatial distribution of motor evoked potentials in an intrinsic hand muscle. Biomed. Tech. (Berl.) 63 (6), 635–645. https://doi.org/10.1515/bmt-2016-0240.

Spampinato, D.A., Ibanez, J., Rocchi, L., Rothwell, J., 2023. Motor potentials evoked by transcranial magnetic stimulation: interpreting a simple measure of a complex system. J. Physiol. 601 (14), 2827–2851. https://doi.org/10.1113/JP281885.

Staudenmann, D., Kingma, I., Daffertshofer, A., Stegeman, D.F., van Dieen, J.H., 2006. Improving EMG-based muscle force estimation by using a high-density EMG grid and principal component analysis. I.E.E.E. Trans. Biomed. Eng. 53 (4), 712–719. https://doi.org/10.1109/TBME.2006.870246.

Stinear, C.M., Barber, P.A., Petoe, M., Anwar, S., Byblow, W.D., 2012. The PREP algorithm predicts potential for upper limb recovery after stroke. Brain 135 (Pt 8), 2527–2535. https://doi.org/10.1093/brain/aws146.

Tankisi, H., Jacobsen, A.B., Fanella, G., Cengiz, B., Kilinc, H., Matamala, J.M., et al., 2025. Short-interval intracortical inhibition and facilitation in amyotrophic lateral sclerosis related to disease phenotype. Clin. Neurophysiol. 176, 2110770. https://doi.org/10.1016/j.clinph.2025.2110770.

Tardelli, G.P., Souza, V.H., Matsuda, R.H., Garcia, M.A.C., Novikov, P.A., Nazarova, M. A., et al., 2022. Forearm and hand muscles exhibit high coactivation and overlapping of cortical motor representations. Brain Topogr. 35 (3), 322–336. https://doi.org/10.1007/s10548-022-00893-1.

Tervo, A.E., Nieminen, J.O., Lioumis, P., Metsomaa, J., Souza, V.H., Sinisalo, H., et al., 2022. Closed-loop optimization of transcranial magnetic stimulation with electroencephalography feedback. Brain Stimul. 15 (2), 523–531. https://doi.org/10.1016/j.brs.2022.01.016.

Traversa, R., Cicinelli, P., Bassi, A., Rossini, P.M., Bernardi, G., 1997. Mapping of motor cortical reorganization after stroke. a brain stimulation study with focal magnetic pulses. Stroke 28 (1), 110–117. https://doi.org/10.1161/01.str.28.1.110.

Tugin, S., Souza, V.H., Nazarova, M.A., Novikov, P.A., Tervo, A.E., Nieminen, J.O., et al., 2021. Effect of stimulus orientation and intensity on short-interval intracortical inhibition (SICI) and facilitation (SICF): a multi-channel transcranial magnetic stimulation study. PLoS One 16 (9), e0257554. https://doi.org/10.1371/journal.pone.0257554.

van de Ruit, M., Grey, M.J., 2016. The TMS map scales with increased stimulation intensity and muscle activation. Brain Topogr. 29 (1), 56–66. https://doi.org/10.1007/s10548-015-0447-1.

van Elswijk, G., Kleine, B.U., Overeem, S., Eshuis, B., Hekkert, K.D., Stegeman, D.F., 2008. Muscle imaging: mapping responses to transcranial magnetic stimulation with high-density surface electromyography. Cortex 44 (5), 609–616. https://doi.org/10.1016/j.cortex.2007.07.003.

Vieira, T.M., Merletti, R., Mesin, L., 2010. Automatic segmentation of surface EMG images: improving the estimation of neuromuscular activity. J. Biomech. 43 (11), 2149–2158. https://doi.org/10.1016/j.jbiomech.2010.03.049.

Volz, L.J., Hamada, M., Rothwell, J.C., Grefkes, C., 2015. What makes the muscle twitch: motor system connectivity and TMS-induced activity. Cereb. Cortex 25 (9), 2346–2353. https://doi.org/10.1093/cercor/bhu032.

Vucic, S., Stanley Chen, K.H., Kiernan, M.C., Hallett, M., Benninger, D.H., Di Lazzaro, V., et al., 2023. Clinical diagnostic utility of transcranial magnetic stimulation in neurological disorders. Updated report of an IFCN committee. Clin. Neurophysiol. 150, 131–175. https://doi.org/10.1016/j.clinph.2023.03.010.

Weise, K., Worbs, T., Kalloch, B., Souza, V.H., Jaquier, A.T., Van Geit, W., et al., 2023. Directional sensitivity of cortical neurons towards TMS-induced electric fields. Imaging Neurosci. (Camb) 1. https://doi.org/10.1162/imag_a_00036.

Ziemann, U., Chen, R., Cohen, L.G., Hallett, M., 1998. Dextromethorphan decreases the excitability of the human motor cortex. Neurology 51 (5), 1320–1324. https://doi.org/10.1212/wnl.51.5.1320.

Ziemann, U., Rothwell, J.C., Ridding, M.C., 1996. Interaction between intracortical inhibition and facilitation in human motor cortex. J Physiol. 496 (Pt 3), 873–881. https://doi.org/10.1113/jphysiol.1996.sp021734.

Ziemann U, Tergau F, Wassermann EM, Wischer S, Hildebrandt J, Paulus W. Demonstration of facilitatory I wave interaction in the human motor cortex by paired transcranial magnetic stimulation. J Physiol. 1998b;511(Pt 1):181-90. 10.1111/j.1469-7793.1998.181bi.x.